RSC Advances

PAPER

View Article Online
View Journal | View Issue

Cite this: *RSC Adv.*, 2021, **11**, 40040

Synthesis, crystal structures, DNA interactions, and antitumor activity of two new dinuclear copper(II) complexes with thiazole ligand†

Zhenfang Zeng, Jiehui Cai, Fuyan Li, Yanying Weng, Qiuping Huang, Honglan Yang, Qiuchan Huang* and Youhuan Wei

Two new dinuclear copper(II) complexes, $[Cu(ambt)_2(cnba)_4]$ (**1**) and $[Cu(ambt)_2(clba)_4]$ (**2**) were synthesized with 2-amino-6-methoxybenzothiazole (ambt) as the main ligand. The structures of the two complexes were characterized by single-crystal XRD. The binding between CT-DNA (calf thymus DNA) and the complexes was evaluated by viscometry, electronic absorption, and fluorescence spectroscopy, and the binding constants were calculated using the Stern–Volmer equation. The complexes were intercalatively bound to CT-DNA, and $[Cu(ambt)_2(clba)_4]$ having a greater binding constant than $[Cu(ambt)_2(cnba)_4]$. The two complexes had better antitumor properties against HepG2 (human hepatocellular carcinoma), A549 (human lung carcinoma), and HeLa (human cervical carcinoma) tumor cell lines than their respective ligands and cisplatin. Furthermore, $[Cu(ambt)_2(clba)_4]$ had a stronger inhibitory ability on the three types of tumor cells than $[Cu(ambt)_2(cnba)_4]$, which is congruent with the binding power of the complexes with DNA. Flow cytometry revealed that $[Cu(ambt)_2(cnba)_4]$ and $[Cu(ambt)_2(clba)_4]$ could trigger apoptosis or necrosis, arrest the HepG2 cell cycles, and cause G0/G1-phase cells to accumulate.

Received 30th July 2021
Accepted 1st December 2021

DOI: 10.1039/d1ra05798g

rsc.li/rsc-advances

1. Introduction

The discovery of cisplatin demonstrated that metal complexes are effective antitumor agents.[1] However, traditional platinum drugs have some side effects including nephrotoxicity and ototoxicity, which limit their clinical application.[2] Transition metal complexes have sparked interest due to their potential applications in antitumor drugs.[3,4] In organisms, DNA is the main genetic material and the carrier of genetic information.[5] It can store and transmit genetic information.[6] Active metal complexes interact with DNA, untwist and bend its double helix, and destroy its structures by covalent binding of specific bases.[7–12] The transition metal represented by copper has excellent coordination properties.[13,14] Meanwhile, copper produces a variable valence ROS (Reactive Oxygen Species) during the transformation from Cu(II) to Cu(I) as a fundamental trace factor for the human body, which can cause tumor cells apoptosis and death.[15–18] Hence, copper complexes are considered as substitute to cisplatin as antitumor drugs.[19–21]

Aromatic carboxylic acids are widely used in the construction of complexes due to their excellent structural rigidity and thermal stability.[22,23] Their carboxyl groups can form monodentate coordination,[24] chelating coordination,[25] and bridging coordination.[26] Metal aromatic carboxylic acid complexes have attracted the attention of researchers due to their unique catalytic activity,[27] optical properties,[28] magnetic properties,[29] and biological properties.[30]

The selection of ligand plays an important role in the biological activity of complexes.[31] Thiazole derivatives, due to their electron donation properties with their nitrogen-containing heterocyclic, are commonly used as dinuclear[32,33] or mononuclear[34] ligands to synthesize multi-functional thiazole metal complexes with transition metal.[35,36] Thiazole metal complexes are widely used in medicine,[37] optical materials,[38] and agriculture.[39] New antitumor drugs may be developed if aromatic carboxylic acid and thiazole are both used as ligands to synthesize copper(II) complexes. For extending this research area further, the synthesis of two new copper(II) complexes with ambt and 4-chloro-3-nitrobenzoic acid (cnba)/4-chlorobenzoic acid (clba) as ligands was reported in this paper. Their structures were characterized through elemental analysis, IR (infrared), as well as X-ray single crystal diffraction. Electronic absorption spectroscopy, fluorescence spectroscopy, and viscosity tests were employed to explore the interactions of the complexes with CT-DNA. According to the data, both complexes were bound to CT-DNA intercalatively. We evaluated the *in vitro* cytotoxicity of $[Cu(ambt)_2(cnba)_4]$ and $[Cu(ambt)_2(clba)_4]$ against HepG2, HeLa, and A549 tumor cell lines by using the CCK-8 assay. The data revealed that the complexes had anti-

School of Chemical and Biological Engineering, Guangxi Normal University for Nationalities, 23 Fozi Road, Chongzuo 532200, PR China. E-mail: huangqiuchan@163.com; weiyouhuan@gxnun.edu.cn; Fax: +86-771-787-0799; Tel: +86-771-787-0799

† Electronic supplementary information (ESI) available. CCDC 2086765 and 2086766. For ESI and crystallographic data in CIF or other electronic format see DOI: 10.1039/d1ra05798g

proliferative activity against the three kinds of tumor cells. Finally, HepG2 cell cycle allocation and apoptosis reaction were examined by flow cytometry in response to exposure to copper(II) complexes. The data suggested that both complexes may induce apoptosis or necrosis.

2. Experimental

2.1. Materials and instrumentation

All reagents of analytical grade were applied without further purification. The Chinese Academy of Council Cell Bank of Typical Culture Preservation (Shanghai, China) supplied the tumor cell lines HepG, HeLa, A549, and LO2. Sinopharm Chemical Reagent Co. Ltd (Shanghai, China) provided all chemicals adopted in this study.

The fluorescence test was carried out on the spectrofluorometer (RF-5301PC, Shimadzu Corp., Kyoto, Japan). Infrared (IR) spectra of the ligands as well as the complexes ranging from 4000–400 cm^{-1} were documented on a FT/IR spectrometer (Spectrum 65, PerkinElmer, Massachusetts, United States) with KBr pellets. Carbon, hydrogen, and nitrogen were quantitated in an elemental analyzer (2400 II, PerkinElmer, Massachusetts, USA), ESI-MS study has been reported on a Time of Flight Mass Spectrometer (G2-XS Tof, Waters Xevo, Massachusetts, USA). Electronic spectra were documented on a spectrophotometer (UV-8000, Yuanxi Corp., Shanghai, China) ranging from 200 to 1100 nm. *In vitro* cytotoxicity assays were carried out on a microplate reader with multiple functions (Multiskan Spectrum, Thermo Fisher Scientific, Massachusetts, USA). Cell cycle and apoptosis assays were carried out in a flow cytometry system (Beckman, CyAn-ADP, California, United States).

2.2. Synthesis

The preparation of complexes was shown in Scheme 1.

2.2.1. Synthesis of $[Cu(ambt)_2(cnba)_4]$ (complex 1). Ambt (0.270 g, 1.5 mmol) and cnba (0.907 g, 4.5 mmol) was mixed and dispersed in 4.0 mL *N*,*N*-dimethylformamide (DMF). A solution of copper(II) nitrate (0.18 mmol) in DMF (10.0 mL) was added to the mixture dropwise. Afterwards, the solution became dark green with a pH of 6.0–7.0. It was stirred for 30 minutes at 25 °C before being sealed with a plastic film and stored in a cool place. Well-formed green crystals that were appropriate for XRD were collected after 20 days with a final yield of 54.7%. The calculated values for $C_{50}H_{42}Cl_4Cu_2N_{10}O_{20}S_2$ (M_w = 1435.94) were 41.82% C; 2.95% H, and 9.75% N, whereas the measured values for $C_{50}H_{42}Cl_4Cu_2N_{10}O_{20}S_2$ were 41.70% C, 2.89% H, and 9.81% N. The IR (cm^{-1}) data was ν(=CH) 3411, ν(=NH) 3149 and 2932, ν(C=C) 1661, 1535 and 780, ν(N=O) 1474, ν(C–N) 1380 and 1218, ν(C–N–C) 1051, 745, and 665, and ν(C–O–C) 921, 830, and 554.

2.2.2. Synthesis of $[Cu(ambt)_2(clba)_4]$ (complex 2). Ambt (0.180 g, 1.0 mmol), as well as clba (0.167 g, 1.0 mmol) were

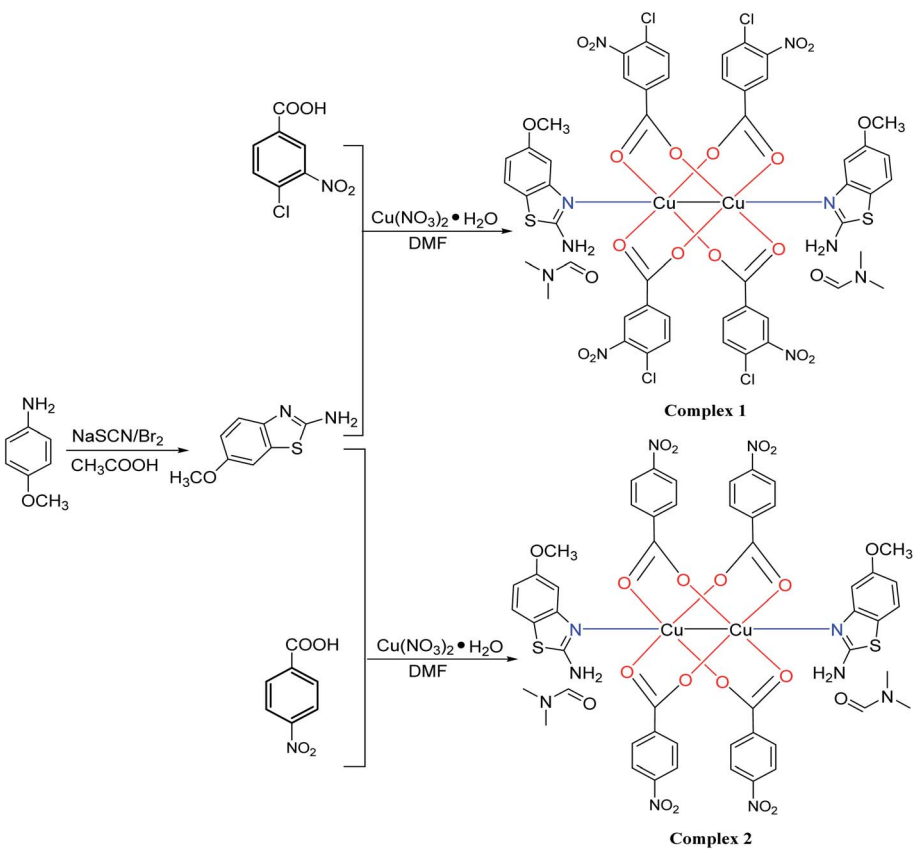

Scheme 1 Synthetic paths for ambt and $[Cu(ambt)_2(cnba)_4]$ and $[Cu(ambt)_2(clba)_4]$.

mixed and dispersed in 10.0 mL DMF. The dissolution of copper(II) nitrate (0.241 g, 1.0 mmol) was made in 5.0 mL of DMF. Copper(II) nitrate solution was slowly put to the mixed solution. After addition, the solution became dark green with a pH of 6.0–6.5. It was stirred for 30 minutes while at 25 °C before being sealed with a plastic film and placed in a cool place. The dark green triangular prism solidified after two months, resulting in well-formed green crystals suitable for XRD. The final yield was 35.13%. The calculated values for $C_{50}H_{46}Cu_2N_{10}O_{20}S_2$ (M_w = 1298.17) were 46.26% C; 3.57% H, and 10.79% N, while the measured values were 46.46% C, 3.61% H, and 10.69% N. The IR (cm^{-1}) data was ν(=CH) 3413, ν(=NH) 3311 and 2935, ν(C=C) 1646, 1597 and 833, ν(N=O) 1521, ν(C–N) 1416 and 1340, 733, ν(C–N–C) 1221, 1058, and 749, and ν(C–O–C) 1100, 1029, and 544.

2.3. Methods

2.3.1. Determination of X-ray structure. Suitable single complex crystals were chosen and installed onto thin glass fibers. The information was gathered for the complexes at 293(2) K with a CCD instrument configured with graphite monochromatic Mo-Kα radiation (λ = 0.71073 Å). The crystal structures were solved by Olex2 and refined by SHELXL-97. The coordinates of the hydrogen atoms were determined by theoretical hydrogenation method. The isotropic and anisotropic temperature factors of hydrogen and non-hydrogen atoms were corrected by full matrix least square approach. Table 1 shows crystallographic and structural refinement data for $[Cu(ambt)_2(cnba)_4]$ and $[Cu(ambt)_2(clba)_4]$. Table S1† shows the chosen bond lengths (Å) along with the angles (°). The Cambridge Crystallographic Data Centre (CCDC) provided crystallographic data at no cost for $[Cu(ambt)_2(cnba)_4]$ and $[Cu(ambt)_2(clba)_4]$. The data is contained in ESI† 2086765 and 2086766.

2.3.2. DNA binding studies. Electronic absorption conveniently explores binding between metal complexes and DNA. The baseline was scanned with Tris–HCl/NaCl buffer solution. We added 2.5 mL complex solution (24 μM for **1** or 12 μM for **2**) and 2.0 mM CT-DNA (30 μL for **1** and 10 μL for **2**) solution were also added into the sample cuvette and the blank cuvette with a pipette gun, respectively. The solution was left to stand for 5 minutes, before being scanned in the wavelength range of 200–450 nm.

The measurement of fluorescence was made on a spectrofluorometer configured with a 1 cm quartz cuvette. A solution of 10.0 mL ethidium bromide (EB, 8 μmol L^{-1}) and 10.0 mL CT-DNA (10 μmol L^{-1}) was allowed to react for 12 h. Afterwards, 2.5 mL EB–CT-DNA mixed solution was added into the sample cuvette. The excitation wavelength and scanning speed were set as 525 nm and 240 nm min^{-1}, respectively. The fluorescence spectrum of the EB–CT-DNA mixed solution at 540–700 nm was determined. To increase the concentration of the complex, a pipette gun was used to slowly add 2 μL of complex solution (50 μM for $[Cu(ambt)_2(cnba)_4]$ or 5 μM for $[Cu(ambt)_2(clba)_4]$) into the EB–CT-DNA mixed system. The solution was mixed thoroughly after each drop and left to stand for 5 minutes to determine the fluorescence emission spectrum.

Table 1 Crystallographic data of $[Cu(ambt)_2(cnba)_4]$ and $[Cu(ambt)_2(clba)_4]$

Complex	$[Cu(ambt)_2(cnba)_4]$	$[Cu(ambt)_2(clba)_4]$
CCDC	2086765	2086766
Empirical formula	$C_{50}H_{42}Cl_4Cu_2N_{10}O_{20}S_2$	$C_{50}H_{46}Cu_2N_{10}O_{20}S_2$
Formula weight	1435.94	1298.17
Temperature (K)	293(2)	293(2)
Wavelength (Å)	0.71073	0.71073
Crystal system	Triclinic	Monoclinic
Space group	$P\bar{1}$	$C2/c$
a (Å)	10.7361(2)	18.4020(3)
b (Å)	12.0568(2)	16.2054(3)
c (Å)	12.4567(2)	18.6394(3)
α (°)	66.295(2)	90
β (°)	81.685(2)	97.992(2)
γ (°)	82.1040(10)	90
Volume ($Å^3$)	1455.27(4)	5504.50(16)
Z	1	4
Dcalcd (Mg m^{-3})	1.638	1.566
μ (mm^{-1})	1.071	0.936
F (000)	730	2664
Crystal size (mm)	0.36 × 0.26 × 0.15	0.32 × 0.20 × 0.18
θ (°)	1.79–25.00	1.68–25.00
Limiting indices	$-12 \le h \le 12$, $-14 \le k \le 14$, $-14 \le l \le 14$	$-21 \le h \le 21$, $-19 \le k \le 19$, $-22 \le l \le 22$
Reflections collected/unique	20 217/5121[R_{int} = 0.0416]	26 762/4857 [R_{int} = 0.0259]
Data/restraints/parameters	5121/0/400	4857/0/382
Goodness-of-fit on F^2	0.820	1.080
Final R indices [I > 2sigma(I)]	R_1 = 0.0293, wR_2 = 0.0954	R_1 = 0.0412, wR_2 = 0.1250
R indices (all data)	R_1 = 0.0333, wR_2 = 0.1001	R_1 = 0.0438, wR_2 = 0.1274
Largest diff. peak and hole (e/$Å^3$)	0.540 and −0.432	1.585 and −0.501

The measurement of CT-DNA relative viscosity was made with an viscometer (Ubbelohde, Shenyi glass Products Co. Ltd, Shanghai, China) at constant 29.0 ± 0.1 °C with and without the complex. The immersion of viscometer was made in the constant temperature water bath for 5 minutes before each measurement was taken. After carrying out each experiment in triplicate, the mean value was taken. The viscometer was filled with 20.0 mL of CT-DNA solution with 200 μM concentration, then the complex solution (1 mM) was gradually added. The [complex]/[DNA] ratio was 0, 0.05, 0.1, 0.15, 0.20, 0.25, 0.30, and the time required for CT-DNA solution to flow through the capillary was recorded. EB was used as a positive control.

2.3.3. *In vitro* cytotoxicity assays. The complexes cytotoxicity against HepG, HeLa, A549, and LO2 cell lines were explored with Cell Counting Kit-8. In brief, HepG, HeLa, A549, and LO2 cells were digested, counted, and prepared into cell suspensions at 5×10^4 cells per mL concentration. Each well of the 96-well cell culture plates was filled with 100 μL cell suspensions (5×10^3 cells per well). The cells were inoculated overnight in a 5% CO_2 incubator at 37 °C. The complete medium (90% medium + 10% fetal bovine serum) was applied to prepare working solution containing complexes at different concentrations. After mixing, 100 μL corresponding working solution were added into each well, and each concentration was triplicated. The 24 hour, 48 hour, 72 hour and 96 hour inoculation of cells were made under 5% CO_2 and 37 °C conditions. The supernatant was discarded and the cells were rinsed once with medium. The cells were cultured continuously for 3 h after 100 μL CCK-8 working solution ($v_{medium} : v_{original\ CCK\text{-}8\ solution} = 10 : 1$) were introduced into each well of the 96-well plates. To calculate the rate of cell proliferation, the OD value ($\lambda = 450$ nm) of each well was determined.

2.3.4. Cell cycle assays. In virtue of the tumor cell cycle, the mechanism of the DNA-binding copper complexes can be identified. The protocol for HepG2 cells of digesting, counting, preparing, and inoculating was similar to that of cytotoxicity assay. After mixing, 2.0 mL corresponding working solution were added into each well. The 24 hour and 48 hour inoculation of cells were made under 5% CO_2 and 37 °C conditions. The cells were washed once using PBS (Phosphate Buffer Saline), digested using trypsin, and centrifuged. The cells were then rinsed twice using precooled PBS. Precooled 70% alcohol was added and cells were fixed and stored at −20 °C. After staining, a Beckman CyAn-ADP flow cytometry platform was used to analyze the samples. The analysis of ten thousand cells was made per sample.

2.3.5. Cell apoptosis assay. The protocol for this experiment was similar to that of cell cycle assay. Cells were collected using centrifugation (1000 rpm min^{-1}) after being digested. We discarded the supernatant and the cells were rinsed twice using 1.0 mL calcium-free PBS. Binding buffer (100 μL), annexin V-FITC (5 μL), along with PI solution (5 μL) were introduced into the plates. The cells were inoculated in the dark at 25 °C for 15 minutes. After adding 400 μL binding buffer, 1×10^4 cells were analyzed at 488 nm with a flow cytometry platform.

3. Results and discussion

3.1. Synthesis and characterization

Two novel dinuclear complexes, $[Cu(ambt)_2(cnba)_4]$ and $[Cu(ambt)_2(clba)_4]$, with ambt as main ligand were synthesized and found to be soluble in DMF and stable in air. The crystallization of $[Cu(ambt)_2(cnba)_4]$ was shown in the triclinic crystal system with space group $P\bar{1}$, however, the crystallization of $[Cu(ambt)_2(clba)_4]$ was shown in the monoclinic crystal system with space group $C2/c$ (Fig. 1). The Cu(II) ions in $[Cu(ambt)_2(cnba)_4]$ and $[Cu(ambt)_2(clba)_4]$ were hexa-coordinated by one oxygen (O) atom from ambt, one Cu(II) atom from the other nuclear, and four oxygen (O) atoms from cnba and clba for $[Cu(ambt)_2(cnba)_4]$ and $[Cu(ambt)_2(clba)_4]$, respectively. The Cu(II)–O distances ranged from 1.9640 (13)–1.9873 (13) and 1.9558 (19)–1.989 (2) Å for $[Cu(ambt)_2(cnba)_4]$ and $[Cu(ambt)_2(clba)_4]$, respectively. The Cu(II)–Cu(II) distance was 2.7290 (4) and 2.6970 (6) for $[Cu(ambt)_2(cnba)_4]$ and $[Cu(ambt)_2(clba)_4]$, respectively. The O/N–Cu–O/N/Cu bond angles ranged from 78.44(4)–172.83(4)° to 81.09(6)–173.01(6)° for $[Cu(ambt)_2(cnba)_4]$ and $[Cu(ambt)_2(clba)_4]$, respectively (Table S1†).

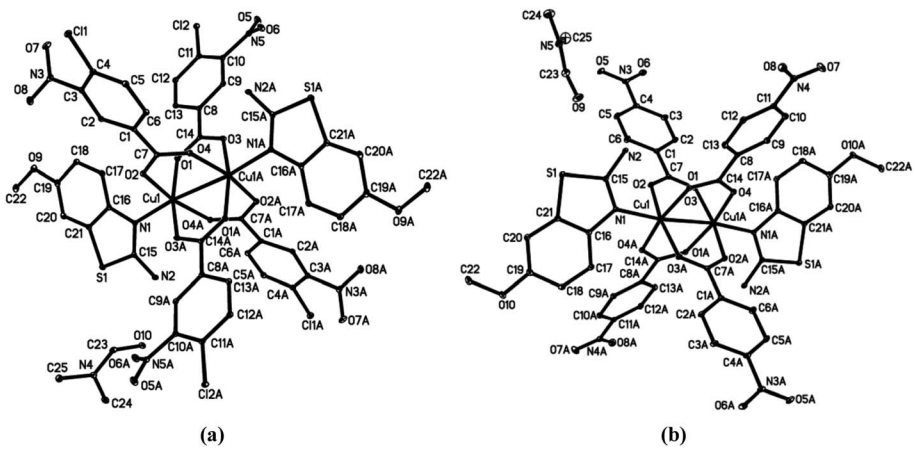

Fig. 1 Crystal structures of $[Cu(ambt)_2(cnba)_4]$ (a) and $[Cu(ambt)_2(clba)_4]$ (b).

ESI-MS spectral study has been performed to determine the composition of the multinuclear two complexes in MeOH (Fig. S5 and S6†). The spectral analyses reveal that $[Cu(ambt)_2(cnba)_4]$ shows m/z value of 1435.6635 (M_w = 1435.94), $[Cu(ambt)_2(clba)_4]$ shows m/z value of 1298.1991 (M_w = 1298.17). These data show that the complexes retain their whole structures in MeOH solution phase.

3.2. DNA binding experiments

3.2.1. Electronic absorption. Electronic absorption is one of the most common, easy, and effective approaches to investigate the interactions between metal complexes and DNA.[40] Phenomenon such as hyperchromicity or hypochromism, redshift or blueshift of the absorption peak of the electronic absorption spectrum, can be employed to assess the binding mode of the complex with DNA due to great stacking interactions between the aromatic chromophore of the benzoyl or thiazole and the DNA base pairs.[41] The electronic absorption peak had hypochromism when the complex interacted with DNA through intercalative binding. However, there was no significant change when the metal complex and DNA were bound in a static or groove surface interaction. The binding strength was analyzed by computing the binding constant (K_b) according to eqn (1):[42]

$$[DNA]/(\varepsilon_a - \varepsilon_f) = [DNA]/[(\varepsilon_b - \varepsilon_f) + 1/K_b(\varepsilon_b - \varepsilon_f)] \quad (1)$$

where ε_a, ε_f, and ε_b mean the appear, free, and bound extinction indicators, respectively. [DNA] means the CT-DNA concentration. K_b represents the ratio of the slope to the intercept. The determined binding constants were 18.8 M^{-1} and 2.04 × 10^4 M^{-1} for $[Cu(ambt)_2(cnba)_4]$ and $[Cu(ambt)_2(clba)_4]$, respectively (Fig. 2). The determined intrinsic equilibrium binding constants (K_b) (10^3–10^5 M^{-1}) conformed to literature values.[43] Thus, the two complexes and the DNA showed high affinity.

3.2.2. Fluorescence spectroscopy. Fluorescence spectrometry is another common approach to assess the binding mode of metal complexes and DNA.[44] In this test, EB was used as a fluorescent probe. The fluorescence performance of the probe was significantly improved when EB was embedded into the base pair of DNA. When the complex solution was introduced to the DNA–EB solution, the fluorescence quenching constant K_{sv} of the complex was computed, and the binding way of the complex with DNA was then analyzed. The fluorescence quenching role of $[Cu(ambt)_2(cnba)_4]$ and $[Cu(ambt)_2(clba)_4]$ on

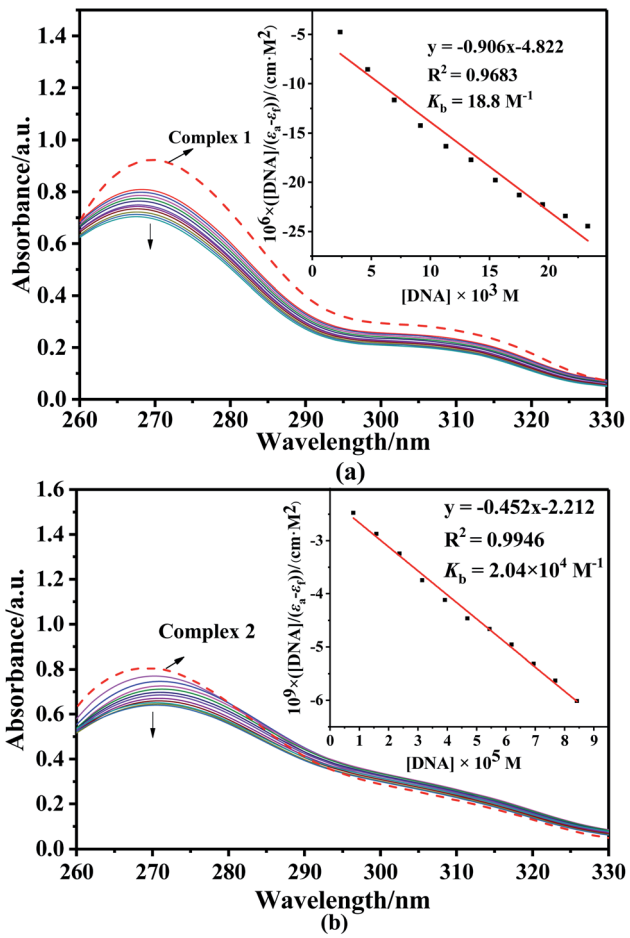

Fig. 2 Electronic absorption spectra of $[Cu(ambt)_2(cnba)_4]$ (a) and $[Cu(ambt)_2(clba)_4]$ (b) in the absence and presence of CT-DNA. Arrows indicate changes in absorbance in response to increasing DNA level. Inset: $[DNA]/(\varepsilon_a - \varepsilon_f)$ *vs.* [DNA] plots.

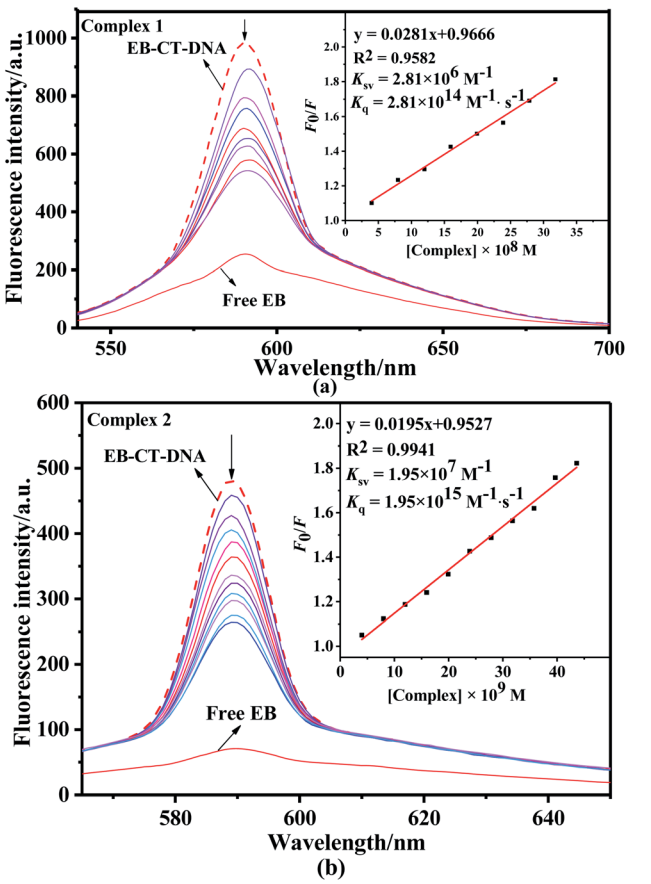

Fig. 3 EB–DNA system emission spectra with and without $[Cu(ambt)_2(cnba)_4]$ (a) and $[Cu(ambt)_2(clba)_4]$ (b). Inset: F_0/F *vs.* [complex] plots. Arrows show variations in intensity as complex concentration escalates.

the EB–CT-DNA system was shown in Fig. 3, and strong fluorescence peaks were notable at 585 nm (Fig. 3a and b). The intensity of fluorescence of the EB–CT-DNA system gradually diminished as complexes were added, and a slight red shift occurred, indicating that complexes may squeeze out EB and enter the DNA base pair through the embedding mode. The classical Stern–Volmer equation was used to quantify the fluorescence quenched by CT-DNA in complexes.[45]

$$F_0/F = 1 + K_q\tau_0[C] = 1 + K_{sv}[C] \quad (2)$$

where F_0 denotes fluorescence intensity as complexes are not added, F means the fluorescence intensity after adding complexes, [C] denotes the concentration of the complex, K_{sv} means the quenching constant, K_q represents the constant rate of bimolecular quenching, and τ_0 represents the lifetime of the fluorescent molecule (almost 10^{-8} s) in the absence of the complex. The F_0/F *vs.* [C] plot is linear, the slope obtained was the quenching constant K_{sv}, and K_q can be obtained by calculation. As shown in Fig. 3, the quenching constants (K_{sv}) were 2.81×10^6 M^{-1} for $[Cu(ambt)_2(cnba)_4]$ and 1.95×10^7 M^{-1} for $[Cu(ambt)_2(clba)_4]$ and $K_{q1} = 2.81 \times 10^{14}$ M^{-1} s^{-1}, $K_{q2} = 1.95 \times 10^{15}$ M^{-1} s^{-1}. The constant rate of quenching (K_q) was evidently greater than the constant restrictive diffusion (K_{dif}) for biomolecules (2.0×10^{10} M^{-1} s^{-1}),[46] showing that the quenching was a static process.[47] Eqn (3) [48] was employed to describe the association of the fluorescence intensity with [C] for static quenching:

$$\log[(F_0 - F)/F] = \log K_a + n \log[C] \quad (3)$$

where n means the quantity of binding places and K_a denotes the association constant. In Fig. 4, the value of K_a was 1.51×10^6 M^{-1} and 2.57×10^8 M^{-1} for $[Cu(ambt)_2(cnba)_4]$ and $[Cu(ambt)_2(clba)_4]$, respectively. The n values were 0.97 and 1.16 for $[Cu(ambt)_2(cnba)_4]$ and $[Cu(ambt)_2(clba)_4]$, respectively.

3.2.3. Viscosity measurements. The viscosity approach is widely regarded as one of the effective methods for researching the interactions between complexes and CT-DNA.[49] The viscosity of CT-DNA solution will not change remarkably if the complex interactions with CT-DNA through the electrostatic, groove binding.[50] Partial or non-classical intercalation bends the CT-DNA helix and decreases DNA viscosity, while classical intercalation increases CT-DNA viscosity.[51] The relative viscosity was obtained by converting the measured time average value according to the following formula (4):[52]

$$\eta = (t - t_0)/t_0 \quad (4)$$

where t_0 designates the time for the buffer solution to flow through the capillary, and t designates the time for the DNA solution containing complex with different concentrations to flow through the capillary. We used $(\eta/\eta_0)^{1/3}$ (η_0 designates the relative viscosity of DNA solution without complex) to [complex]/[DNA]. The viscosity of DNA increases as the [complex]/[DNA] ratio rise (Fig. 5). Therefore, copper(II) complex binds DNA by intercalation as EB. Absorption and emission spectrum analysis corroborated this conclusion.

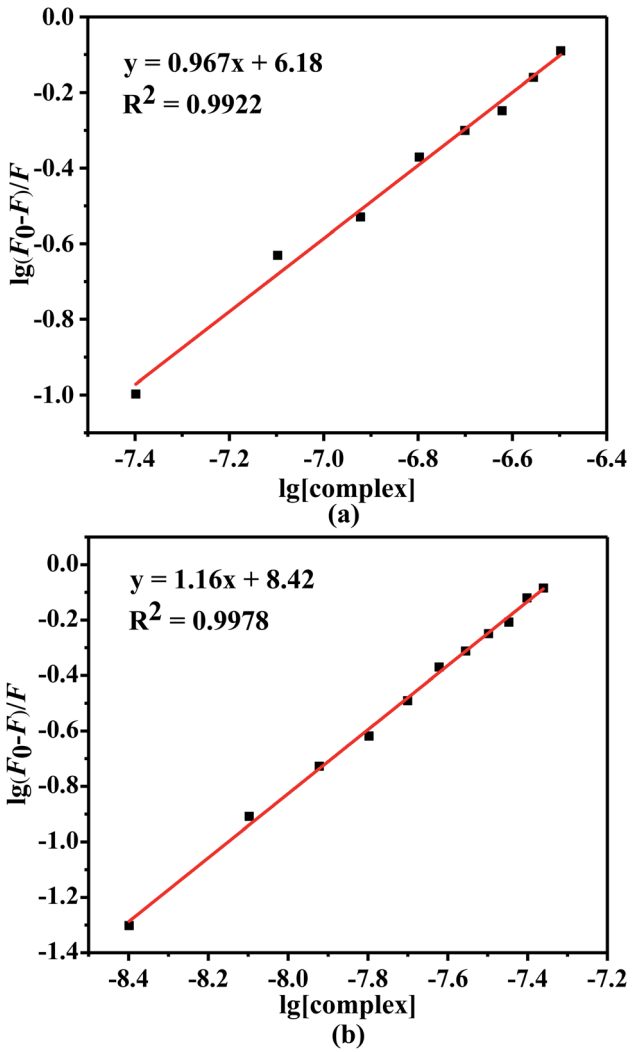

Fig. 4 Double-log plots of CT-DNA fluorescence quenching by $[Cu(ambt)_2(cnba)_4]$ (a) and $[Cu(ambt)_2(clba)_4]$ (b).

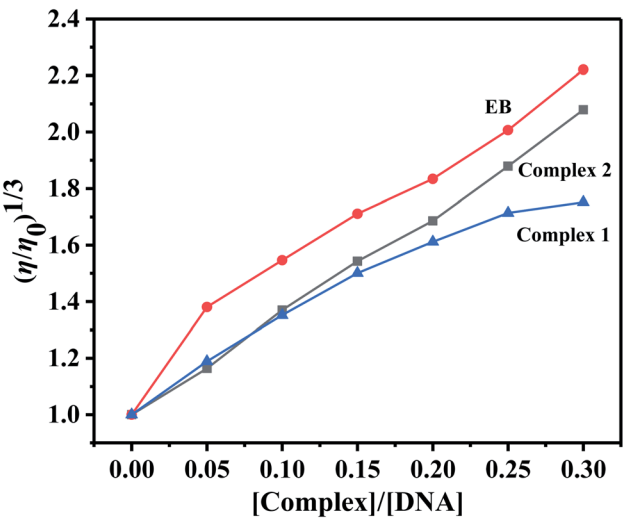

Fig. 5 Increasing number of the complex and EB had an effect on related CT-DNA viscosity.

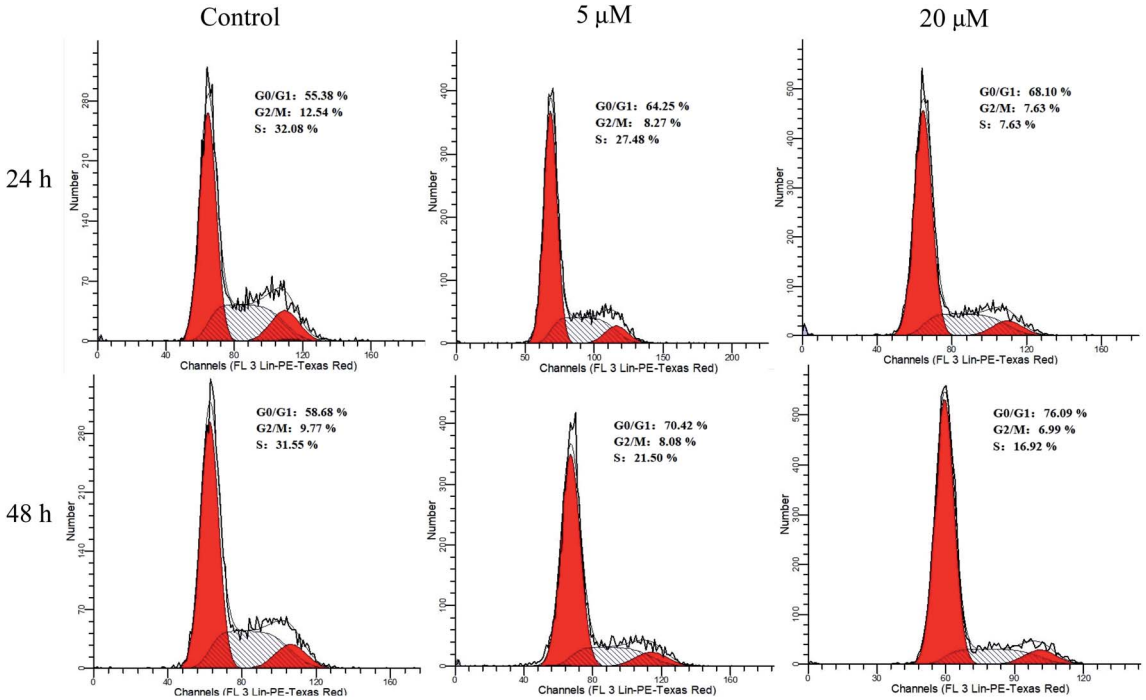

Fig. 6 Distribution of HepG2 cell cycle after 24 h and 48 h exposure to $[Cu(ambt)_2(cnba)_4]$.

3.3. Cytotoxicity assay *in vitro*

The cell lines HepG, HeLa, A549, and LO2 were inoculated with diverse levels of $[Cu(ambt)_2(cnba)_4]$ and $[Cu(ambt)_2(clba)_4]$ for 24 h, 48 h, 72 h, and 96 h. The effects of complexes on HepG, HeLa, A549, and LO2 cells viability and proliferation were shown in Fig. 6 and 7. The IC_{50} of complexes against HepG, HeLa, A549, and LO2 cells at different time points were shown in Table 2. These data illustrated that both the complexes had strong anti-proliferative activity against HepG, HeLa, A549 cells. At the same time point, both complexes had greater antitumor efficacy against three kinds tumor cell lines than the ligands

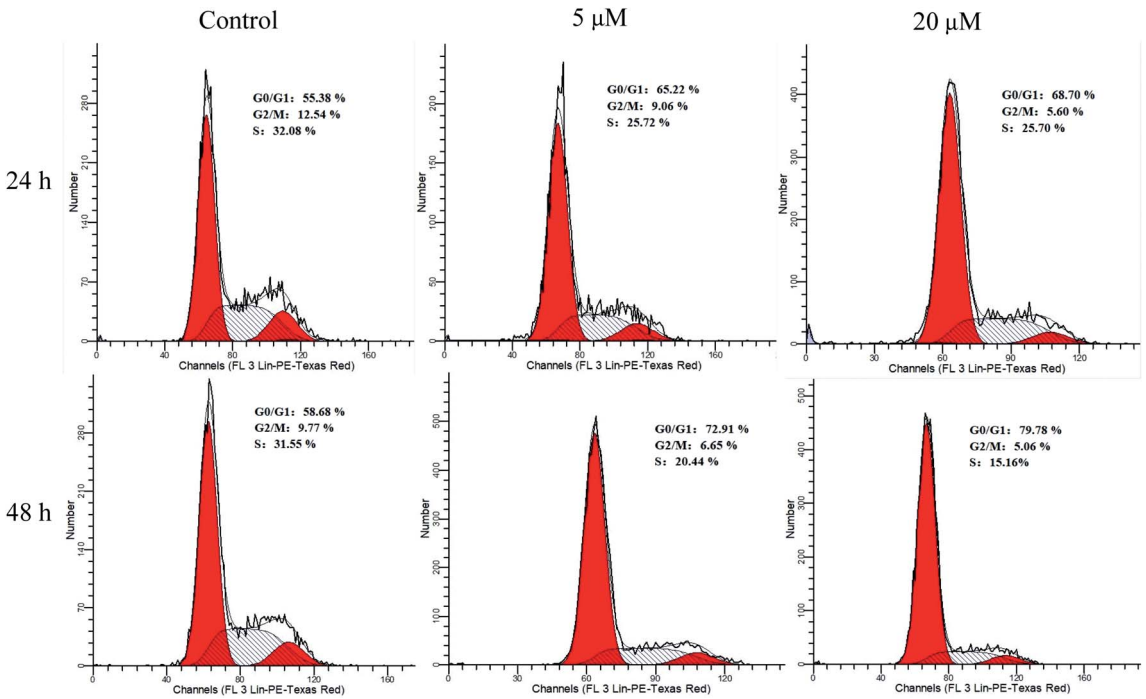

Fig. 7 Distribution of HepG2 cell cycle after 24 h and 48 h exposure to $[Cu(ambt)_2(clba)_4]$.

Table 2 Value of IC_{50} of the complexes against HepG, HeLa, A549, and LO2 at various time points

	IC_{50} (μM)				
Complexes	*t* (h)	LO2	A549	HeLa	HepG2
1	24	87.41 ± 1.94	61.56 ± 1.08	37.27 ± 1.05	48.35 ± 0.86
	48	50.28 ± 1.70	25.73 ± 0.79	19.77 ± 1.03	23.47 ± 0.85
	72	26.62 ± 1.43	20.39 ± 0.85	11.85 ± 0.95	14.56 ± 0.87
	96	14.74 ± 0.93	11.80 ± 0.78	7.43 ± 0.74	9.31 ± 0.79
2	24	92.86 ± 1.97	36.94 ± 1.12	21.85 ± 0.86	29.84 ± 0.86
	48	53.22 ± 1.73	25.13 ± 1.01	14.58 ± 0.76	14.97 ± 0.74
	72	29.20 ± 1.47	19.96 ± 1.00	11.59 ± 0.77	11.57 ± 0.75
	96	17.74 ± 1.25	9.86 ± 0.86	1.86 ± 0.53	7.75 ± 0.70
Anba	48	>1000	975.4 ± 1.76	>1000	>1,000,0
Ambt	48	>10 000	>10 000	>10 000	>1000
Clba	48	>10 000	>10 000	>1000	>1000
Cisplatin	48	37.34 ± 1.57	36.50 ± 1.76	37.37 ± 2.01	43.81 ± 1.62

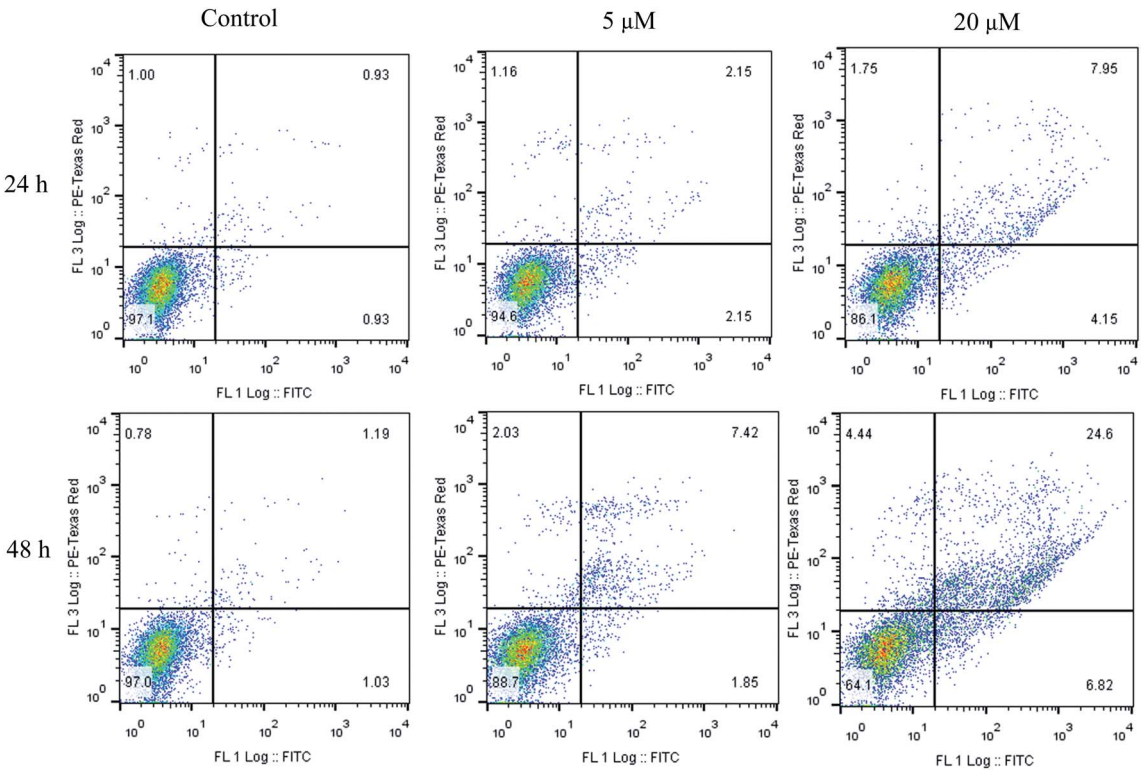

Fig. 8 HepG2 cells were inoculated with various levels of $[Cu(ambt)_2(cnba)_4]$ for different durations.

and the positive control cisplatin but lower efficacy against LO2. However, $[Cu(ambt)_2(clba)_4]$ had a stronger activity than $[Cu(ambt)_2(cnba)_4]$. Cell viability was concentration- and time-dependent, indicating that both complexes gradually entered the cells and caused apoptosis.

3.4. Cell cycle arrest

The distribution of HepG2 cells across various stages of the cell cycle was explored by flow cytometry and PI staining. The proportions of HepG2 cells at G0/G1 were 55.38% at 24 h (Fig. 6) and 58.68% at 48 h (Fig. 7). After incubation with complexes **1** or **2** to the time point, the proportion of G0/G1 phase increased, whereas the proportion of G2/M and S phase declined. Compared with the control, $[Cu(ambt)_2(cnba)_4]$ and $[Cu(ambt)_2(clba)_4]$ triggered G0/G1 stage arrest in HepG2 cells, and the proportion of G0/G1 phase was concentration- and time-reliance, with $[Cu(ambt)_2(clba)_4]$ showing a stronger activity than $[Cu(ambt)_2(cnba)_4]$.

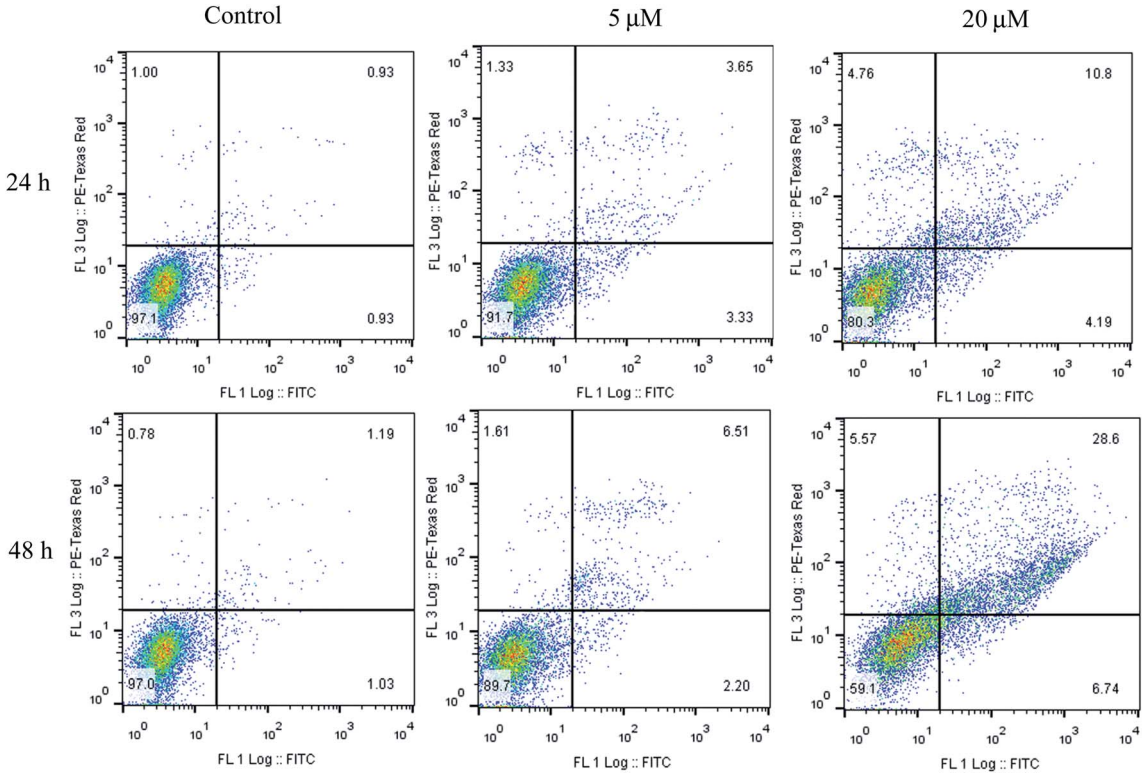

Fig. 9 HepG2 cells were inoculated with various levels of $[Cu(ambt)_2(clba)_4]$ for different durations).

3.5. Cell apoptosis assay

With untreated HepG2 cells served as control, flow cytometry investigated the apoptosis in HepG2 cells (Fig. 8 and 9). After exposing the copper(II) complexes with 5 μM and 20 μM to the cells for 24 hours, the ratios of apoptotic or necrosis cells were 5.4% and 13.9% for $[Cu(ambt)_2(cnba)_4]$ while 8.3% and 19.7% for $[Cu(ambt)_2(clba)_4]$. The ratios of apoptotic or necrosis cells for the control was 2.9%. After 48 hour exposure to the same conditions, the ratios of apoptotic or necrosis cells were 11.3% and 35.9% for $[Cu(ambt)_2(cnba)_4]$ while 10.3% and 40.9% for $[Cu(ambt)_2(clba)_4]$. The ratios of apoptotic or necrosis cells for the control was 3.0%. By comparing with the control, the ratio of living cells had declined while that of apoptotic or necrosis cells had grown in $[Cu(ambt)_2(cnba)_4]$ and $[Cu(ambt)_2(clba)_4]$ treatments, and $[Cu(ambt)_2(clba)_4]$ exhibited a stronger activity on apoptosis activity against HepG cells. The apoptotic or necrosis effect of the copper(II) complexes on the HepG2 cells was both concentration- and time-dependent.

4. Conclusions

Herein, two new copper dinuclear complexes were synthesized with ambt as the main ligand. Both complexes had copper binuclear coordination structures. $[Cu(ambt)_2(cnba)_4]$ was triclinic system with $P\bar{1}$ space group while $[Cu(ambt)_2(clba)_4]$ was monoclinic system with $C2/c$ space group. Both $[Cu(ambt)_2(cnba)_4]$ and $[Cu(ambt)_2(clba)_4]$ bound intercalatively to DNA and $[Cu(ambt)_2(clba)_4]$ showed greater binding constant than $[Cu(ambt)_2(cnba)_4]$. The fluorescence quenching of $[Cu(ambt)_2(cnba)_4]$ and $[Cu(ambt)_2(clba)_4]$ to CT-DNA was static quenching. Compared with ligands and cisplatin, the complexes had stronger anti-proliferative activity against HepG2, A549, and HeLa tumor cells. The inhibitory ability of $[Cu(ambt)_2(clba)_4]$ on the three kinds of tumor cells was stronger. This is congruent with the binding power of $[Cu(ambt)_2(cnba)_4]$ and $[Cu(ambt)_2(clba)_4]$ with DNA, indicating that the antitumor movement of the complexes may be linked to their binding ability with DNA. $[Cu(ambt)_2(cnba)_4]$ and $[Cu(ambt)_2(clba)_4]$ inhibit tumor cells by inducing apoptosis or necrosis in HepG2 cells, and arresting HepG2 cell cycle in G0/G1 phase. This work may aid in the development of Cu(II) complexes as potential antitumor reagents in the future.

Author contributions

Zhenfang Zeng: designed the methodology and drafted the original manuscript. Jiehui Cai: performed the experiments. Qiuping Huang: conceptualized the whole research. Yanying Weng: performed data curation. Qiuchan Huang: drafted and edited the manuscript. Youhuan Wei: drafted and reviewed the manuscript as well as sourced for funding.

Conflicts of interest

The authors report no conflicts of interest.

Acknowledgements

The work was funded by the Middle-aged and Young Teachers' Basic Ability Promotion Project of Guangxi (No. 2017KY0846 and 2019KY0769), the Scientific Research Project of Guangxi Normal University for Nationalities (No. 1011/3270020101, 327003070414, 327003070416, 327002060107, 31700702, 2019YB018, and 2020GP008).

References

1 L. Qi, Q. Luo, Y. Zhang, F. Jia and F. Wang, *Chem. Res. Toxicol.*, 2019, **32**, 1469–1486.
2 S. Hosseinzadeh, M. E. Moghadam, S. Sheshmani and A. S. Shahvelayati, *J. Biomol. Struct. Dyn.*, 2019, 2215–2228.
3 B. Q. Zou, X. L. Huang, Q. P. Qin, Z. F. Wang and H. Liang, *Polyhedron*, 2020, **181**, 114482.
4 J. Alday, A. M. Mazzeo and S. Suarez, *Inorg. Chim. Acta*, 2020, **510**, 119696.
5 S. Pereira, *Am. J. Bioeth.*, 2019, **19**, 75–76.
6 H. H. Lee, R. Kalhor, N. Goela, J. Bolot and G. M. Church, *Nat. Commun.*, 2019, **10**, 2383–2394.
7 S. S. A. Fathima, R. Paulpandiyan and E. R. Nagarajan, *J. Mol. Struct.*, 2019, **1178**, 179–191.
8 S. Elleuchi, I. O. D. Luzuriaga, N. Sanchez-Gonzalez, X. Lopez and A. Gil, *Inorg. Chem.*, 2020, **59**, 12711–12721.
9 P. J. Jarman, F. Noakes, S. Fairbanks, K. Smitten, I. K. Griffiths, H. K. Saeed, J. A. Thomas and C. Smythe, *J. Am. Chem. Soc.*, 2019, **141**, 2925–2937.
10 Z. Yaghobi, Z. R. Ranjbar and S. Gharbi, *Polyhedron*, 2019, **164**, 176–184.
11 G. Barone, A. Terenzi, A. Lauria, A. M. Almerico, J. M. Leal, N. Busto and B. Garcia, *Coord. Chem. Rev.*, 2013, **257**, 2848–2862.
12 L. Antonino, B. Riccardo, T. Alessio, S. Angelo, G. Francesco, L. Alessandro, A. A. Maria and B. Giampaolo, *Dalton Trans.*, 2014, **43**, 6108–6119.
13 C. Zhang, C. Huang, S. Wei, X. Cai and A. A. Pimerzine, *Thermochim. Acta*, 2020, **690**, 178661–178667.
14 J. Wang, X. P. Zhou, Q. Lv and H. L. Yuan, *J. Mol. Struct.*, 2021, **1231**, 129964–129970.
15 C. J. Nunes, A. H. Otake, S. O. Bustos, R. B. Fazzi and A. Ferreira, *Chem.–Biol. Interact.*, 2019, **311**, 108789.
16 T. Shen, X. X. Hu, Y. Liu, Y. Zhang and X. B. Zhang, *ACS Appl. Mater. Interfaces*, 2020, **12**, 5403–5412.
17 A. Zafar, S. Singh, S. Ahmad, S. Khan, M. I. Siddiqi and I. Naseem, *Bioorg. Chem.*, 2019, **87**, 276–290.
18 S. Karpagam, R. Kartikeyan, P. P. Nachiyar, M. Velusamy and M. Kannan, *J. Coord. Chem.*, 2019, 3102–3127.
19 M. Ociepa, S. Bakalarz, M. Nentwig, O. Oeckler, M. Gajewska, E. Turlej, J. Wietrzyk and D. Michalska, *Inorg. Chim. Acta*, 2019, **490**, 68–77.
20 S. Jiang, H. Ni, F. Liu, S. Gu and Y. Gou, *Inorg. Chim. Acta*, 2019, **499**, 119186–119195.
21 G. L. Chang, Z. Li, M. J. Niu and S. N. Wang, *J. Coord. Chem.*, 2019, **72**, 2422–2436.
22 F. Y. Ju and S. Li, *Russ. J. Gen. Chem.*, 2020, **90**, 1083–1087.
23 X. Wang, M. Kong, D. Li, J. Fang, Z. Deng and H. Zhang, *Crystengcomm*, 2019, **21**, 2144–2153.
24 M. M. Zhu, J. Cui, Y. L. Zeng, N. Ren and J. J. Zhang, *Polyhedron*, 2019, **158**, 485–493.
25 L. N. Zhu, Z. P. Deng, S. W. Ng, L. H. Huo and S. Gao, *Dalton Trans.*, 2019, **48**, 7589–7601.
26 F. Y. Jie, C. Y. I. Ping, G. X. Mei, H. H. Bing and G. Z. Hui, *J. Mol. Struct.*, 2019, **1195**, 929–935.
27 M. Bakir, M. W. Lawrence, P. Nelson and M. B. Yamin, *J. Coord. Chem.*, 2019, **72**, 2261–2278.
28 K. B. Manjunatha, R. Rajarao, P. Poornesh, B. J. Rudresha, G. Umesh and B. R. Bhat, *Opt. Mater.*, 2019, **89**, 494–497.
29 P. Thanakit, D. Limthin, P. Leepheng, S. Suramitr and D. Phromyothin, *Ferroelectrics*, 2019, **552**, 108–120.
30 T. Madanhire, H. Davids, M. C. Pereira, E. C. Hosten and A. R. Abrahams, *Polyhedron*, 2020, **185**, 114583.
31 W. H. El-Shwiniy, L. M. Abbass, S. A. Sadeek and W. A. Zordok, *Russ. J. Gen. Chem.*, 2020, **90**, 483–488.
32 N. Alvarez, F. Velluti, F. Guidali, G. Serra and M. H. T. vz, *Inorg. Chim. Acta*, 2020, **508**, 119622.
33 H. Kotani, D. Hong, K. Satonaka, T. Ishizuka and T. Kojima, *Inorg. Chem.*, 2019, **58**, 3676–3682.
34 S. R. Shah, Z. Shah, M. Khiat, S. A. Halim, A. Khan, J. Hussain, R. Csuk, M. U. Anwar and A. Al-Harrasi, *Appl. Organomet. Chem.*, 2020, **34**, e5842.
35 M. Kaufmann, C. Müller, A. A. Cullen, M. P. Brandon and M. T. Pryce, *Inorg. Chem.*, 2020, **60**, 760–773.
36 S. Safaei, J. Wang and P. C. Junk, *J. Solid State Chem.*, 2020, **294**, 121762–1121773.
37 A. M. Khedr, H. El-Ghamry, M. A. Kassem, F. A. Saad and N. El-Guesmi, *Inorg. Chem. Commun.*, 2019, **108**, 107496.
38 J. Zhao, X. Chen, J. Wu, M. Jian and Z. Chi, *J. Mater. Chem. C*, 2020, **8**, 10390–10400.
39 B. H. Pursuwani, B. S. Bhatt, F. U. Vaidya, C. Pathak and M. N. Patel, *J. Biomol. Struct. Dyn.*, 2020, **39**, 1–12.
40 N. Ning, D. Q. Zhao, H. Li, J. Nan, J. Y. Wen and H. Y. Liu, *Molecules*, 2015, **21**, 54.
41 H. W. Mo, Y. X. Liu, D. H. Cai, F. Shen and X. Y. Le, *Chin. J. Inorg. Chem.*, 2019, **35**, 477–484.
42 V. N. Kadam, K. Saikrishnan and K. N. Ganesh, *J. Phys. Chem. C*, 2018, **122**, 14004–14013.
43 A. Draksharapu, A. Boersma, M. Leising, A. Meetsma, W. R. Browne and G. Roelfes, *Dalton Trans.*, 2015, **44**, 3647–3655.
44 C. L. Zhang, Y. X. Liu, X. M. Zhang, S. Chen, F. Shen, Y. H. Xiong, W. Liu, Z. W. Mao and X. Y. Le, *Mater. Sci. Eng. C*, 2018, **91**, 414–425.
45 T. Sohrabi, M. Hosseinzadeh, S. Beigoli, M. R. Saberi and J. Chamani, *J. Mol. Liq.*, 2018, **256**, 127–138.
46 Y. Zhang, J. Y. Wen, M. H. Mahmood, X. L. Wang, B. B. Lv, X. Ying, H. Wang, L. N. Ji and H. Y. Liu, *Luminescence*, 2015, **30**, 1045–1054.
47 G. Zhang and Y. Ma, *Food Chem.*, 2013, **136**, 446–449.
48 B. H. Pursuwani, B. S. Bhatt, F. U. Vaidya, C. Pathak and M. N. Patel, *J. Fluoresc.*, 2021, **31**, 349–362.
49 A. A. Hassan, A. A. Aly, N. K. Mohamed, K. M. E. Shaieb, M. M. Makhlouf, E. S. M. N. Abdelhafez, S. Brase,

M. Nieger, K. N. Dalby and T. S. Kaoud, *Bioorg. Chem.*, 2019, **85**, 585–599.
50 N. Vamsikrishna, M. P. Kumar, G. Ramesh, N. Ganji, S. Daravath and Shivaraj, *J. Chem. Sci.*, 2017, **129**, 609–622.
51 B. Anupama, *J. Mol. Struct.*, 2020, **1210**, 127988.
52 Z. F. Zeng, Q. P. Huang, J. H. Cai, G. J. Zheng, Q. C. Huang, Z. L. Liu, Z. L. Chen and Y. H. Wei, *Molecules*, 2021, **26**, 4028.